THEORY, DESIGN, AND DEVELOPMENT OF AN OPEN-SOURCE 3D PRINTED PERISTALTIC PUMP FOR MICROFLUIDICS APPLICATIONS

By

Joshua M. MacEachern, B.S.

A Thesis Submitted in Partial Fulfillment of the Requirements

for the Degree of

Master of Science

in

Mechanical Engineering

University of Alaska Fairbanks

May 2022

Approved:

Cheng-fu Chen, Committee Chair
Rorik Peterson, Committee Co-Chair
Daisy Huang, Committee Member
Bernard Laughlin, Committee Member
Rorik Peterson, Chair
Department of Mechanical Engineering
William Schnabel, Dean
College of Engineering and Mines
Richard Collins, *Director of the Graduate School*

ABSTRACT

Microfluidics research is a constantly evolving and developing field of research in the biological, chemical, and medical sciences. To perform microfluidic analyses, various types of pump designs have been developed or optimized. These pumps are generally capable of pumping flow in the range of 0.1-100s of microliters (μL) per minute, with the goal of pumping fluid with an extremely consistent flow rate. These pumps include, but are not limited to, peristaltic, syringe, membrane, and lobe pumps. Both commercial and open-source designs have been developed to meet the needs of continued research. Commercial designs are very expensive, but offer limited flexibility to tailor the usage for custom assays. Open-source designs that have been presented may lack support, or may be designed to use fabrication technologies that are less commonly available than conventional desktop 3D printing. Due to this, many laboratories may be limited in their microfluidic research work due to either availability of commercial pumps, or usability of open-source pump designs. This work presents two iterations of a novel design for a 3D-printable microfluidic peristaltic pump. The pumps developed herein have been tested to demonstrate consistent performance operating over long-term periods of up to ten days continuously. These pumps have been tested to demonstrate capability of delivering aqueous flow as slow as flow ranges of 10s of μL/min. These pumps are capable of maintaining an outlet pressure of up to 220 kilopascals (kPa). In a tube of 1 mm inner diameter, this pressure would drive a flow rate of 10 μL/min through tubing up to 6.6 meters long. Finally, this design has been optimized to improve the user experience and make these peristaltic pumps both easy to maintain and easy to operate by a non-technical user.

TABLE OF CONTENTS

LIST OF FIGURES

Page

List of Tables

CHAPTER 1. INTRODUCTION

Microfluidics devices and lab-on-a-chip systems are a widely used and well-known workflow in research fields such as analytical chemistry, pharmaceutical development, and neurobiology [1]. Microfluidic analyses have a variety of advantages over conventional counterpoints, namely the lower price, smaller sample volumes, faster reaction rates, and overall, a smaller, more readily usable size [2]. However, one of the largest barriers to entry for research in these fields is initial capital costs. To solve this issue, many researchers turn towards Open-Source Hardware (OSHW) that can be readily made with inexpensive equipment such as desktop 3-D printers [3]. OSHW is valuable not just because it is freely accessible and reproducible, but also it is extremely easy to modify existing designs [4]. These features of OSHW allow for laboratory equipment to be made and modified to fit the needs of individual users, without being constrained by the manufacturer's limited hardware or software offerings. In this thesis, a work based on OSHW for prototyping precision pumps for microfluidic usage is presented.

There are two primary types of pumps used in microfluidic devices: syringe pumps and peristaltic pumps. The basic construction of a syringe pump consists of a controllable linear actuator, which pushes the plunger of a syringe. The primary advantage of syringe pumps is their extremely smooth flow regime; however, the limited reservoir volume tends to be a deterrent for many applications. Additionally, the syringe material compatibility must be considered for the liquid being pumped, and the liquid cannot generally contain suspended solids, or slurries.

Peristaltic pumps operate by compressing a flexible or semiflexible tube with a series of rollers, or wipers. They are a kind of positive displacement pump which operates by applying pressure to the fluid itself. Once the tube relaxes after a roller passes it, it re-expands, which draws new fluid into the tubing. One of the most common materials used for tubing is high-

purity silicone, which is commonly available in a variety of sizes and is extremely chemically inert. Peristaltic pumps tend to be desirable for many applications because the only thing that comes in contact with the pumped fluid is the tubing itself, and no pump components.

Due to the method of operation, peristaltic pumps are very resilient, and can pump extremely viscous liquids and slurries with fewer issues than syringe pumps. They can also pump an indefinite volume from any size reservoir. The trade-off of this flexibility, however, is that the flow is characteristically pulsatile. Rather than having smooth, continuous flow, the rollers push the liquid in pulses that are approximately the volume of the tube between each roller. Peristaltic pumps may be configured in one of two ways: "open" flow, where liquids are pumped from a main fluid reservoir that may be refilled, or "closed" flow, where the liquid being pumped is recirculated [5]. In the closed flow configuration, the outlet of the pump is connected to the inlet, with process tubing and equipment between the two.

Peristaltic pumps capable of microfluidic-level flow rates are used in a variety of fields, including biology, chemistry, pharmaceuticals, and environmental research. Biologically, micropumps are frequently used in research on gene chips and capillary electrophoresis [6]. In chemical synthesis, microfluids pumps have become a relatively common tool. Chemical reactions that are performed within microfluidic reactors tend to be both faster and safer, and they are often used for research involving highly reactive, toxic, or explosive intermediates [7]. The lower volume allows for these reactions to go to completion without potentially disastrous results.

Peristaltic pumps for laboratory-scale research are available from a variety of manufacturers such as Lambda, Fisher Scientific, and MEINHARD. These commercial pumps generally fall into two categories: extremely precise pumps that have a limited maximum flow rate, or less

precise pumps that may pump a broad range of flow rates. Pumps are available at resolutions down to 0.2 μL/min, but these pumps have a maximum flow rate of only 60 μL/min. Pumps in the range of a 1 μL/min resolution may achieve flow rates as high as 50 mL/min. Although commercial pumps would meet the needs of most if not all research, the cost tends to be extremely high. For example, a single 4-channel pump from MEINHARD has a base price of $2,400 [8]. If multiple experiments need to be conducted simultaneously, this cost point would be prohibitive for many projects. The goal of this work is to match or improve the performance of the commercial pumps that have a lower resolution and a high flow-rate range. The second goal of this work is to match or improve the cost of microfluidic pumps, making research in this field more readily available.

Peristaltic pumps can also be customer-made in house with rapid prototyping techniques such as 3D printing. Multiple designs for open-source 3D printable peristaltic pumps have been demonstrated previously. Many of these designs have used one large roller over which multiple hoses are stretched. This enables multi-channel pumping, but all pumps will output the same flow rate [9], [10]. This may be advantageous for assays where multiple tests are being conducted simultaneously but suffers from the inability to control each flow individually. Among those 3D printed pumps, some designs use more commonly available Fused-Filament-Fabrication (FFF) 3D printers, but encounter the same challenges presented in this work, namely the unsatisfactory resolution of the printed parts and anisotropy of part strengths. To avoid the issues of FFF 3D printed parts, other designs adopt resin-based 3D printing.

Resin-based stereolithography (SLA) offers a higher accuracy than FFF 3D prints. The most common form of SLA 3D printing is masked stereolithography, or mSLA. However, this less common technique imposes different challenges than FFF 3D printing. The technique of mSLA

involves the use of toxic resins, which are both messy and more expensive in comparison to FFF thermoplastic. Resin-based 3D prints also must be washed in isopropyl alcohol and then post cured under UV light [11].This additional step in the workflow is not necessarily a problem, but it adds additional complexity and workspace to handle the hazardous resin. Parts that are made via mSLA demonstrate a higher resolution and improved isotropy over parts made with FFF. Figure 1 shows two open-source 3D printable peristaltic microfluids pumps, with Figure 1(a) showing a pump produced with FFF printing and Figure 1(b) showing a pump produced with mSLA printing.

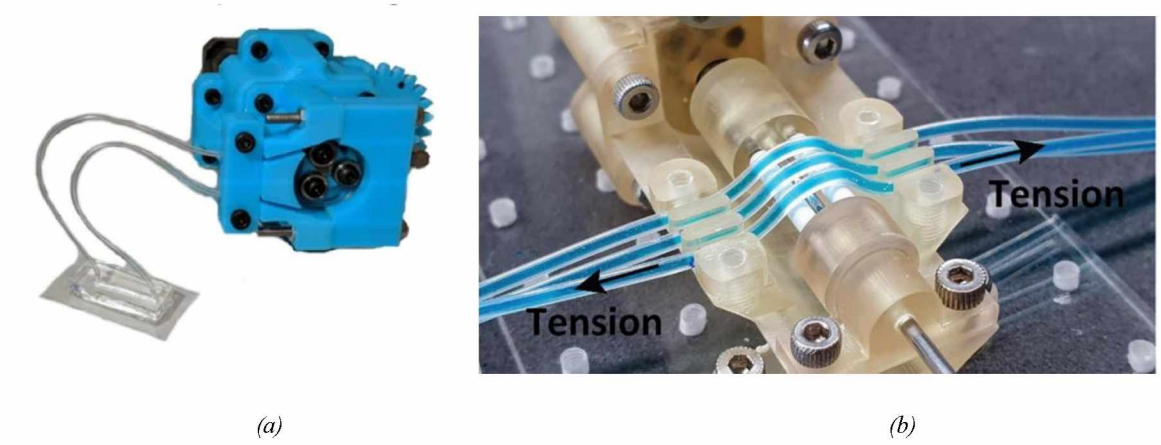

(a) *(b)*

Figure 1: Example Open-Source Peristaltic Pumps. A) Behrens et. al; B) Ching et al.

An observable trend is that pumps created with FFF methods generally have a gear reduction that is used to provide more torque to turn the rotors and are generally not capable of extremely low flow rates [12] In contrast, pumps designed to be manufactured with mSLA are generally able to directly drive such low flow rates without additional hardware such as ball bearings [10]. In FFF parts, however, a thread form may be cut, or a threaded insert may be installed to allow for consistent and reliable fastening. The photopolymer resin used in mSLA is more brittle and inserts can not be melted in, so adding fasteners to these prints requires a more careful design process.

The slow flow rates required to reduce the backpressure at the microfluids scale make the development of macro-scale hardware for micro-scale fluids challenging. At a slow flow regime, surface tension plays a major role in dictating the fluid behavior [13]. Additionally, the resistance to flow increases drastically as a function of the length of tubing and the square of the fluid velocity [14]. Due to the extremely small diameter of microchannels in common assays, pressure drop in these channels may be extremely high [15]. The relative surface roughness of microchannels is high enough that continuous flow is severely limited by the back pressure of the channels [16]. For this reason, most microfluidic analysis tends to stay in the laminar or creeping flow regions. At these flow regimes, manufacturing tolerances on peristaltic pumps play an important role, in that if the occlusion of the pump is too low, fluid will be able to flow backwards through it. The occlusion of a peristaltic pump can be described as the distance between the two walls of the tubing as it is compressed.

$$Occ = 1 - \frac{r_b - r_{roller} - r_{offset} - 2h}{2r_{in}} \quad \text{Eq. 1}$$

$$h = r_o - r_{in} \quad \text{Eq. 2}$$

Eq. 1 gives an expression of the occlusion of a peristaltic pump, where r_b is the radius from the central axis of the pump to the wall of the pump, r_{roller} is the radius of the rollers themselves, r_{offset} is the distance from the center of the rollers to the wall of the pump, and h is the wall thickness of the tubing. The wall thickness is defined by Eq. 2 where r_o is the outer diameter of the pump tubing and r_{in} is the inner diameter of the tubing [17]. A zero or low occlusion pump will be capable of a higher output pressure but will reduce the tubing longevity. Higher occlusion pumps will reduce wear on the tubing, but flow will be able to slip back through the pump.

The existing work in both commercial and open-source microfluids pumps still has areas that can be improved. Commercial pumps remain too expensive for many research teams to

effectively utilize. Open-source designs for FFF-produced microfluids pumps often are bulky and have exposed workings. These exposed gears may provide both a safety risk to the users and to the hardware itself. Finally, designs that exist for SLA printing are limited in their flow rate range, and the longevity of the parts is limited by the materials utilized. The open-source designs addressed in this work all lack a simple programming interface, as well. They can be programmed to pump at a specific speed, but flow patterns or timed flow is often not feasible. This work explores the hardware design and development, as well as the testing and validation of an open-source peristaltic pump referred to as the Open-Source Multichannel Microfluidics (OSMM) pump.

CHAPTER 2. INITIAL PROTOTYPE OF 3D PRINTED PERISTALTIC PUMPS

The development of the initial prototype was intended as an early proof of concept. The feasibility of 3D printed microfluidic pumps with fused deposition modeling (FDM) prints was not widely documented, and any demonstration of microfluidic capability was desirable. Once the initial design had been tested and determined to be feasible, then it could be improved upon. This prototype was designed to be produced with both mSLA and FFF 3D printing. Once the prototype had been tested to demonstrate its functionality, it was presented to other research groups to get feedback on feasibility. Ultimately, much of this early pump design is deprecated but it provided valuable information in the development of a second version.

2.1 Hardware Description

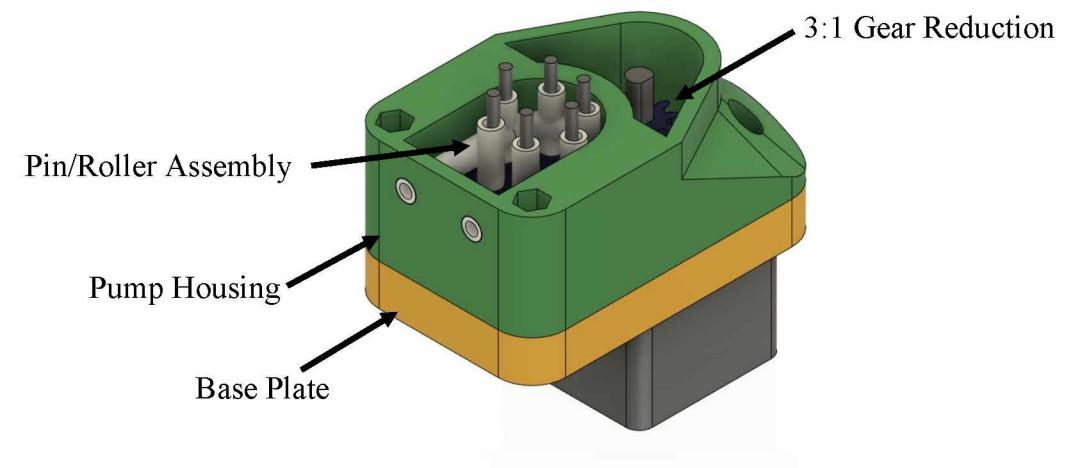

Figure 2: Three-Quarter Render View of Version 1 OSMM Pump

Figure 2 shows the original design of the pump. It consists of a base plate (yellow), a FFF printed gear reduction (blue), the pins and roller assembly (gray/white), and the pump housing (green). The baseplate is mounted directly to the faceplate holes of the motor, and the shaft for the roller gear is pressed directly into it. The pump was designed around the relatively small, but

readily available NEMA 14 stepper motor. These steppers are available in a variety of specifications for power demands and accuracy, but the motors chosen have a precision of 1.8° per step, and a torque output of 23 N-cm.

Herringbone gears of gear ratio 3:1 were 3D-printed to further increase the torque. The primary consideration of the gears was printability on a FFF 3D printer. Although SLA printers produce much more detailed and accurate parts, the resin utilized tends to be brittle, making it not ideal for load-bearing applications such as the gears. Due to the restriction of printability on FDM, a relatively large module for the gears was chosen to improve the mechanical toughness of the printed gears.

The initial designs utilized fixed steel pins to press against the tubing to produce the needed flow for pumping, as shown in Figure 3. However, this initial design was not a viable option as explained below. The friction between the pins and the tubing can be is extremely high, which caused the selected NEMA 14 motor to stall at all speeds. When turned manually, the friction on the tubing also caused the tubing to be pushed out of the path of the pins. Finally, the small diameter of the pins caused pinching and wear of the silicone tubing used for the pumping action. The larger diameter of the rollers caused the force of the roller to be spread over a larger area and eliminated any creasing of the tubes.

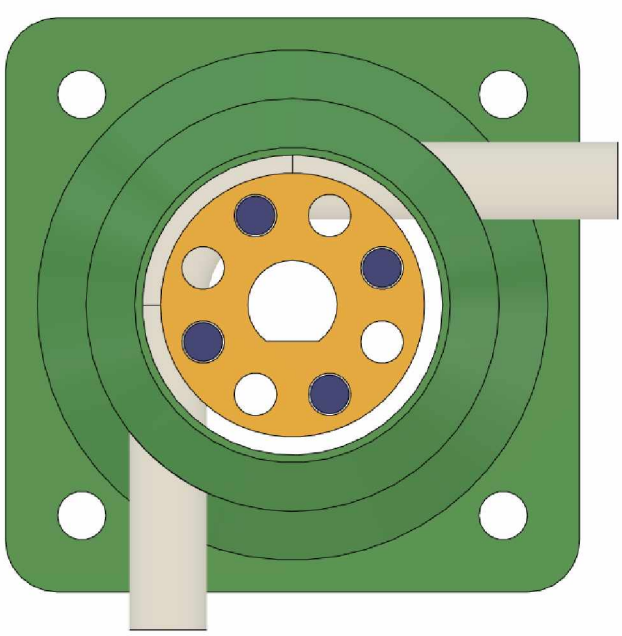

Figure 3: Diagram of initial model showing pins (blue), casing (green), pin holder (yellow), and hose (white)

To overcome the friction issue, the initial design was modified to use rollers instead of simple fixed pins. This design is conventionally used in design and manufacturing of peristaltic pumps. Commercial rollers generally use either metal or high-end polymers for their roller construction, but this option is undesirable due to the cost. For this reason, alternative roller options were pursued in this thesis.

A few options for making cost-effective rollers were explored in this work: FDM printed rollers, PTFE tubing-based rollers, and polyamide(nylon) screw standoffs-based rollers. Of these options, the only ones that were determined to be feasible were the nylon screw standoffs. The other roller ideas are presented here but were not ultimately used due to consistency issues as detailed below.

Early roller concepts were made to be 3D printed, but due to poor rolling characteristics and inconsistent walls, a different methodology was required. For use in a peristaltic pump, the diameter of a roller is required to be extremely consistent, but the wall thickness of thin FDM

prints that are relatively small (less than 4mm) tends to be inconsistent. Furthermore, the 3D printed rollers would bind on the pins, causing the pumps to stall from the friction between the rollers and the tube. Finally, FFF 3D prints will have a seam line where each layer of the print begins and ends. This seam line became a problem as it drastically affected the rollers' roundness. An example seam line on a 3D print is seen in Figure 4 below.

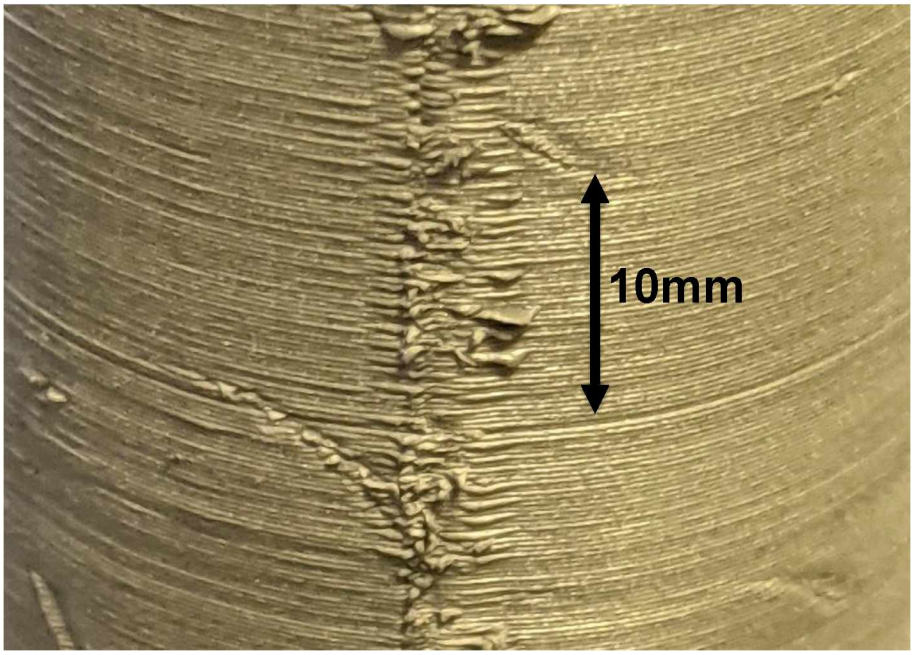

Figure 4: Wall inconsistencies due to seams in FFF printed part

Using polytetrafluoroethylene (PTFE, commonly known as Teflon) tubing intended for 3D printing filament tubes was explored as an inexpensive potential material to create the rollers. This tubing comes in sizes that are generally approximately 1.9 mm internal diameter (ID) and 4 mm outer diameter (OD) [18]. Rollers were constructed by simply cutting this material to length, but the wall thickness varied by up to 0.5 mm. This variance in wall thickness was intolerable for the application of rollers, due to the fact that this would cause a variation in the occlusion of the pumps, and therefore this path was abandoned.

Eventually, commercially available polyamide (Nylon) screw standoffs were chosen for the rollers. The wall thickness of these rollers is very consistent, and the unlubricated friction coefficient between Nylon and the steel dowel pins used for the shafts is relatively low at 0.4 [19]. In many applications, the need to have a sterile and/or clean environment precludes the use of lubrication, particularly on exposed components. Due to this, use of an unlubricated or dry system is preferred. Nylon is an acceptable material for applications where a material may encounter chemicals; this resin is considered to be chemically inert and will not negatively react to inorganic solvents [20]. These standoffs are also available in a variety of materials including stainless steel, aluminum, Low-density polyethylene (LDPE), and zinc-plated brass. One major goal during the development of this project was to decrease the prohibitively high cost barrier to entry, which made these nylon standoffs an obvious choice due to their low unit cost. The standoffs chosen for this project were purchased from McMaster-Carr, and a pack of 100 standoffs was purchased for $10.60 USD. This breaks down to approximately ¢11 each, or a roller cost of only $0.66 per pump.

For chemical contact peristaltic pumps, the most common tubing material chosen is high-purity silicone. This silicone can withstand both high temperatures and most chemical compounds. The tubing chosen had an OD of 3 mm and ID of 1.5 mm. This size was chosen initially for its ready availability, but this is not a very desirable size of tubing for this application. The primary issue with this tubing selection is that it is not compatible with most commonly available sizes of connectors. It is too small for many barb connectors, and too large for most probe needle type connections [21]. The smallest needle size that would fit this tubing well is a 14-gauge needle, which are on the large side for microfluids applications. For this

reason, the tubing in the second version was changed to a larger size compatible with more commonly available barb connectors.

2.2 Design for Manufacturing with mSLA 3D Printers

This pump design was designed to be entirely 3D printed on a standard FDM machine, such as a Creality Ender-3 or a Prusa i3 Mk. 3. The models created for production of these first-generation pumps were developed to limit the need for support structures, which is a scaffolding geometry constructed by FDM machines to support overhangs.

Once initial designs had been constructed it found that the original geometry of designs was less precise than needed for producing the required details with an FDM machine. Rather than attempting to compensate for the inherent imprecision of FDM 3D printers, the parts were modified to be printed on a masked-Stereolithography(mSLA) 3D printer. These printers tend to be significantly more precise than FDM 3D printers and allow much higher resolution prints to be produced. This additional resolution was able to compensate for the other, less accurate FDM printed parts, and allowed for the prototype to be able to pump more effectively. The design was further refined and optimized to utilize the SLA printing method. Due to the differences in how FFF and mSLA 3D printers operate, the parts optimized for SLA printing are challenging to print on an FFF machine. Figure 5 shows a completed prototype pump. The translucent, whitish cover has been SLA printed, but the solid white gears and pump base could handle lower tolerances and were printed on an FDM printer instead.

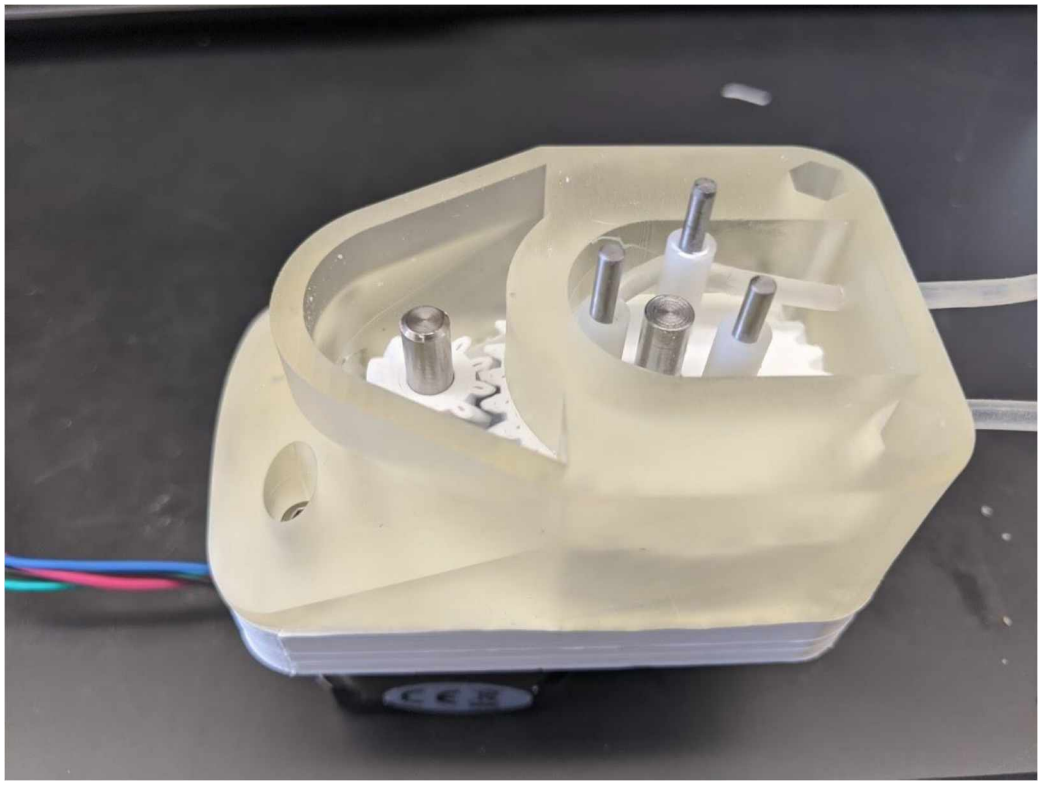

Figure 5: Image of completed prototype pump

2.3 Electronics and Firmware

Simple control of the pumps was desirable, and for this reason, 3D printer control boards were the most obvious choice. They already provide ready support for a variety of stepper motor drivers, and there are many open-source firmware options that are well supported. Additionally, due to the established 3D printer hobbyist community, it is easy to find support for these control boards that would be much more challenging with a custom solution.

2.3.1 RAMPS 1.4 Control Board

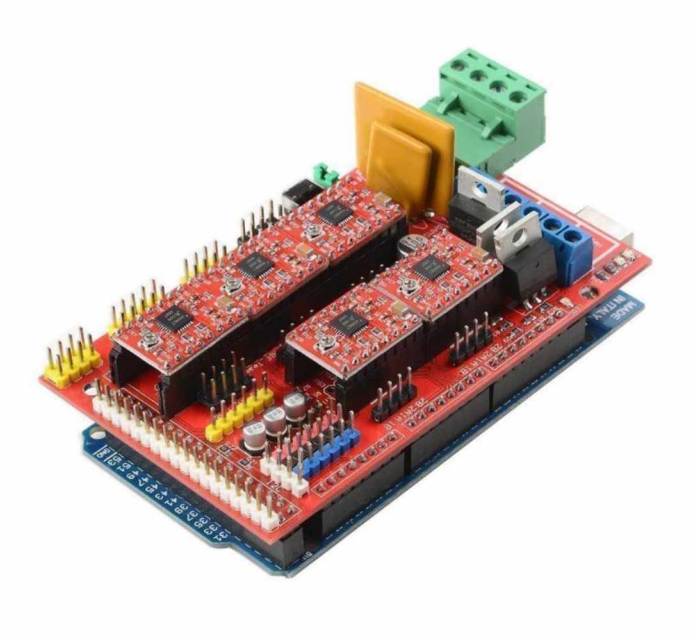

Figure 6: RAMPS 1.4 and Arduino Mega

The RepRap Arduino Mega Pololu Shield (RAMPS) version 1.4 was chosen for the initial prototype due to its ease of use and its low cost. The RAMPS board design consists of a shield with connectors for controlling up to five stepper motors and drivers. It utilizes the Arduino Mega 2560 platform for control and processing, with an 8-bit Atmel Atmega 2560 processor. The RAMPS shield itself was designed as a low-cost solution to fit the entire electronics needed for a RepRap 3D printer into a small package [22]. The design is modular and includes plug-in stepper drivers that, in this case, were used to control up to five individual motors. An Arduino Mega with a RAMPS 1.4 shield installed is shown in Figure 6.

However, this design with the RAMPS controller has significant limitations when used for extended periods of time for numerous small movements. The 8-bit processor can readily be overloaded by incoming commands, which causes stuttering to the motors as it has to pause to process commands. Additionally, it does not have built-in support or SPI bridges that could be

utilized for higher quality stepper drivers such as the Trinamic TMC2130, which limits its precision unless the motherboard wiring is reconfigured for this missing functionality. The design also takes up a significant amount of vertical space, as it consists of an Arduino mega, with the RAMPS daughterboard on top of that, and a display daughterboard on top of the RAMPS board.

2.3.2 Allegro A4988

The Allegro A4988 is a micro stepping stepper motor driver with a built-in logic translator for easy operation. The A4988 is capable for up to one-sixteenth step microstep operation, and the output can be used for up to 2A motor current. The Allegro A4988 became popular in the 3D printing world with the development of the "StepStick" board, as an A4988 breakout board which became the de-facto standard for utilization in replaceable stepper driver boards. A StepStick board with an A4988 chip is shown in Figure 7. It was developed by RepRap forum user "Joem" and released on 18 March 2011 [23]. This stepper driver was selected initially due to its low cost and wide availability, as well as being able to readily slot into the RAMPS control board that was chosen. One major challenge with the A4988 StepSticks is the current adjustment method. In order to set the current that is being sent to the motors, a potentiometer has to be manually adjusted while measuring a reference voltage. This can be tedious, and needs to be done any time the motors are changed. If this is not done, or is done incorrectly, it can cause the motors to overheat, or the output torque to be severely limited.

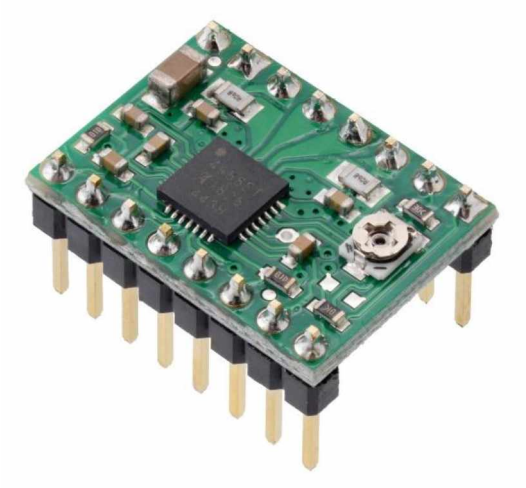

Figure 7: Allegro A4988 stepper motor driver in "StepStick" form factor

The price point of the A4988 stepper drivers shows in high performance applications though. They are both electrically and physically noisy during operation. When they are used to hold a motor in a position, a high-pitched whine emanates from them, and is annoying to work around consistently. The electrical noise may interfere with sensors and data collection for microfluids, and so separation of the pumps and the sensors is necessary. The A4988 is an old control chip, and does not offer a lot of features that more sophisticated drivers may have such as stall detection, overheat protection, or software adjustable current settings.

2.3.3 Marlin Firmware

Since the RAMPS board was designed to be used to control a 3D printer, a commonly available open-source firmware was chosen. Two of the most developed open-source 3D printer firmware are Marlin and Klipper. Marlin is a firmware that was initially intended for the RepRap family of 3D printer designs. The firmware is developed by a team of developers with a goal to be “a straightforward, reliable, and adaptable printer driver that ‘just works.’” The Klipper firmware is another relatively common option. Klipper developers advertise that it can print

faster and more accurately, but it does this by performing the strenuous calculations on a Raspberry Pi. The added cost of using a Raspberry Pi was not desirable for these prototypes. Additionally, the desired flow rate of these pumps is extremely slow, so the performance boost at high speeds is not necessary. Other than simplicity, the primary reason that Marlin firmware was chosen was due to its very thorough hardware abstraction layer (HAL), which allows the same configuration files to be used for both 8-bit development boards (such as the RAMPS board) and 32-bit development boards, such as the SKR 2. In order to modify the firmware such that it is compatible with both control boards presented in this thesis, only a single line of the original code needs to be modified in a configuration file. This functionality allows for rapid changes to be made to the electronics configuration, both between generational changes of the OSMM Pump architecture, and to accommodate for users to use a different control board with the same pump system.

2.3.4 Controller System

Figure 8: OSMM Pump Control Box

To improve user experience and reduce risk to electronics, a controller box was designed. This unit contained the power supply necessary for the pumps, as well as the control board and LCD controller screen. This unit also provided mounting for up to five pumps (the maximum that could be individually controlled with this controller). Figure 8 shows the control unit with four pumps mounted to it (one slot was empty at the time of testing). Not all the pumps are fully assembled in the image, but everything else is functional. This control unit *worked*, but it needed a thorough redesign to improve user experience and reduce risk to the electronics should a pump fail. The control unit allowed for access to the SD card slot to load files to the pump on the side,

as well as access to control the pump over a serial connection to a computer at the rear of the box.

2.4 Results

As this pump design test was solely intended as a proof of concept, testing was not extremely thorough. Much of the testing relied on qualitative impressions of how the pump felt to use and interact with. This pump demonstrated enough lab feasibility to warrant getting user feedback. As potential users interacted with the pump system, enough deficiencies were seen to justify an almost complete redesign. Due to this, the user interactions were seen as the most valuable information about this first version.

2.4.1 Feasibility and Reliability Testing

One of the primary issues with the first version of successful prototypes was consistency of the pumps, and as such, the testing focused on improving that. To establish the pump behavior in different flow rate regimes, a characteristic curve showing the output volume as a function of the rotational speed was created, as seen in Figure 9. The maximum speed the pump could operate at before stalling the motor was established as the 100% speed, and the speed values were normalized to that. During these tests, the duration was adjusted to maintain a theoretically identical dispensed volume. Eq. *3* describes the inverse relationship between a change in volume ΔV(µL) and a time duration t(min) to maintain a constant volume flow rate Q(µL/min.)

$$Q = \frac{\Delta V}{t} \qquad \text{Eq. 3}$$

During this test, the pumps had not been calibrated. In order to calibrate the pumps, a relation between the steps of the motor, and the output volume needs to be established. If the pumps are perfectly consistent, a horizontal line would be expected, meaning the output volumetric flow

rate is consistent for all speeds from 0-100%. Additionally, if individual pumps were consistent between each other, it would be expected to see them all follow the same horizontal line. Figure 9 demonstrates a high level of similarity between pumps A and B but shows that pump C had a lower volume output consistently. This may be either due to a manufacturing inconsistency, or a warped part as described in the following chapter.

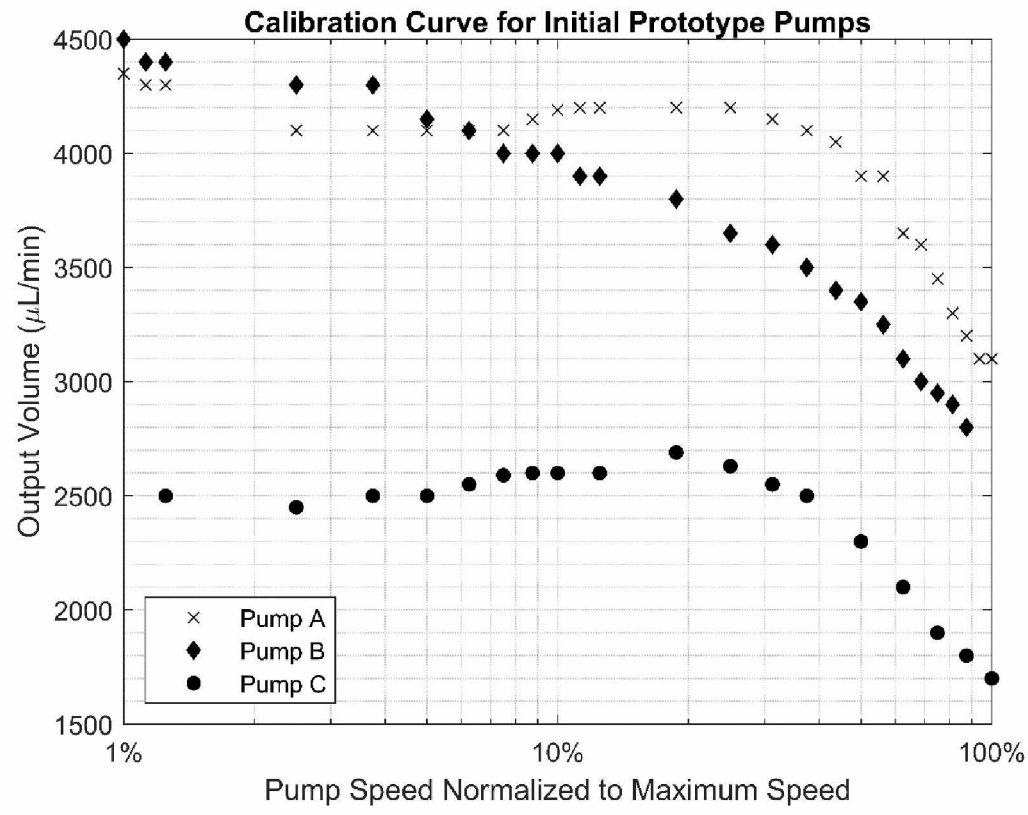

Figure 9: Pump Speed vs. Dispensed Volume for Version 1 OSMM pumps

The data in Figure 9 shows a wide flat linear region of pump flow between 0.7 and 25% for pumps A and C with a very significant drop-off in output volume at the high end of the tested region. Pump B demonstrates a much more consistently linear decay trend than the other two pumps. This is likely due to the tubing used not being stiff enough to expand back to an uncompressed state before the next roller re-compresses it. Due to this, the pump fails to produce the same output per pulse and the flow quickly drops off enough to be ineffective. This

inconsistency at higher speeds is highly undesirable, as the effective useful flow rates of the pump are restricted to the linear range. Additionally, the backpressure in the tubing becomes significant at higher flow rates. This would cause a significant drop in the outlet pressure of the pumps, and thus the flow rate. Section 4.3.3 addresses this problem in detail, as the second iteration of the pump prototypes were more thoroughly tested.

2.4.2 User Experience

To further evaluate performance of the system, the prototyped pump system was presented to multiple teams working on a variety of research projects at the University of Alaska-Fairbanks.

The overall response to the pumps was satisfactory; however, there were multiple concerns in the operation and feasibility of the design. The primary concern was with how the tube was mounted and fixed. This pump system simply used a frictional fit between the tubing and the body of the pump, meaning that the holes modelled into the side of the pump unit for the tube inlet and outlet were undersized relative to the tubing outer diameter. This proved to be challenging to change and was an obvious candidate for improvement in the second version.

In addition to the tubing being challenging to change, this pump design had other deficiencies which would preclude it from being used for biological research. Due to the pump construction, it could not readily be sterilized. This lack of sterilization would mean that either a newly constructed pump would need to be used for every experiment, or, more likely, this pump would not be used at all. Additionally, the lack of common fittings made integration challenging. Many research environments already have specific fitting interconnections that they would like to make. Due to this design using an uncommon size of tubing, connecting a standard fitting to it is more challenging.

2.5 Summary of Design Deficiencies of the Initial Design

The most obvious place for improvement in the user experience of OSMM Pump version 1 was in the tubing mounting method. Since the tubing was only fixed by a friction fit against circular holes, the tubing tended to slip. Additionally, to change worn pump tubing out for new, fresh tubing, the system required that the user pull out the old tubing through the entire pump mechanism. Fresh tubing was installed by cutting the end of the tube at a sharp angle, which allowed the tube to be fed through the inlet hole. The user would then use a pair of tweezers or sharp needle nose-type pliers to pull the tube through that hole. The tube was then pushed around the rollers while the pump needed to be turning, and finally was pulled/pushed through the outlet hole in the body. This was not only extremely tedious, but it also had a high potential to contaminate the tubing.

The next most obvious place to improve the design was in how power was delivered from the motor to the roller gear. In this first design, the pressure from the tubing pushed on the rollers and caused warping of the driven gear. This affected long-term reliability and consistency of the pumps, and preventing this cantilever effect was desirable for a second version. Additionally, this first design simply uses a slip fit between the driven gear and its axle. This not only affected its consistency due to imprecise rolling, it also tended to wear relatively quickly. The pressure on the axle caused the hole to slowly grow larger, which decreased the amount of pressure on the tubing dramatically.

Finally, the largest area for improvement in the user experience of this initial design was in the programming of the pumps. Scripts had been written that were compatible with MATLAB/Octave that could generate machine code compatible with the control units, but they were slow, unintuitive, and required users to have MATLAB or Octave available.

2.6 Outlook for Improved Design

This initial prototype design was treated mostly as a proof of concept. Once it was shown that the pumps *could* pump effectively, work began on the second version OSMM pump. Since OSMM pump v2.0 was developed during the testing phase of OSMM pump v1.0, the testing for the first version was not extremely thorough and was instead treated as a proof of concept. The version 2.0 prototype consisted of a comprehensive redesign and would need to be completely tested all over again to characterize its flow behavior. In order to improve the design, three major areas of improvement were identified: The pump/tube connection and interface, the power delivery, and the programming methods.

CHAPTER 3. IMPROVED DESIGN (VERSION 2)

3.1 Notable Changes in Design

The most significant change to the design between the first and second version of the peristaltic pump prototype involves the adoption of a cartridge for the tubing to be mounted in. These cartridges accept standard Luer-lock fittings and allow for easy changing of the tubing. Additionally, the design for the tubing cartridge is fully parameterized in the CAD software. This allows for a new cartridge model to be made for different size tubing, without needing to remodel the entire cartridge. Additionally, the occlusion of the pump may also be changed with these parameters, allowing for different stiffnesses of tubing to be readily used. The power delivery mechanism was changed to reduce cantilever effects. Finally, a new program was written in Python to program the pumps more easily. The new design of both the control box and the pumps is shown in Figure 10.

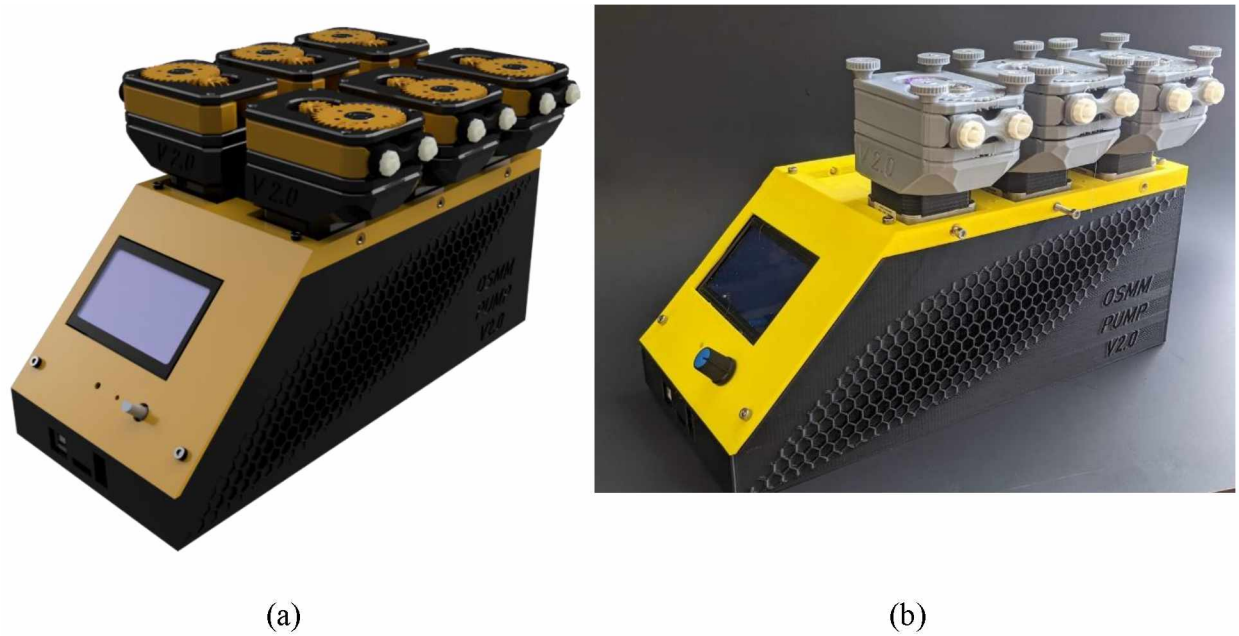

(a) (b)

Figure 10: CAD Render of Version 2 Control Box and Pumps (a) and Actual Printed Control Box and 3 Pumps (b)

3.1.1 The Use of Standard Luer-Lock FittingsIn the first version of the OSMM Pump system, it was determined through user feedback that the method of mounting the pump tubing in place was effective, but it lacked ease of use, especially when changing tubing. Not only was this methodology highly finicky, requiring very careful attention to detail, but it also tended to damage the tubing. The pulling of the tubing tended to stretch it excessively, which would cause premature wear to the tubing itself. Additionally, due to the ends of the tubing not being fixed, they could generate large amounts of strain at the inlet and exit.

The soft tubing used also did not have any sort of readily available connector or fitting that allowed for tubing interoperability. Although fittings could be used with the tubing originally designed for, it was an uncommonly used standard size of tubing, and there was no way of fixing the fittings to the pump body. This led to the decision of using the standard Luer-lock fittings for the second major version of the prototype.

ISO 80369-7 governs the use and geometry of Luer-lock connectors, which are widely used in both medical and research applications [24]. Luer-lock connectors may be designed to have a variety of fitting sizes available for different tubing. The male and female connectors are all a standard size, but the inlet and outlet to these fittings varies to accommodate most tubing up to ½". The flexibility that this interoperability allows for is further increased through the fact that many needles, IV fluid bags, and syringes use the Luer-lock standard. This allows for sterility to be maintained in a closed system with these pumps, without having to adapt through multiple fittings. In any fluid system where sterility is important, decreasing the number of fittings that the fluid must pass through tends to benefit the application as each fitting provides further points where bacterial development and/or flow recirculation may occur.

One of the key challenges with the first version of the pump was both the lack of fittings, and the challenge of changing the tubing. For this reason, a new approach needed to be taken with this second version. Additionally, some design changes needed to be made to hold the ends of the tubing in place. For this reason, design of the pumps lent itself toward a cartridge-based design, which is detailed below.

3.2 Tubing Cartridge Design

As described above, the tubing interchangeability was very poor due to the friction fit used. In order to accommodate this problem, a cartridge was designed for the tubing to be easily interchanged. This cartridge design is shown in Figure 11, and shown in cross-section in Figure 12.

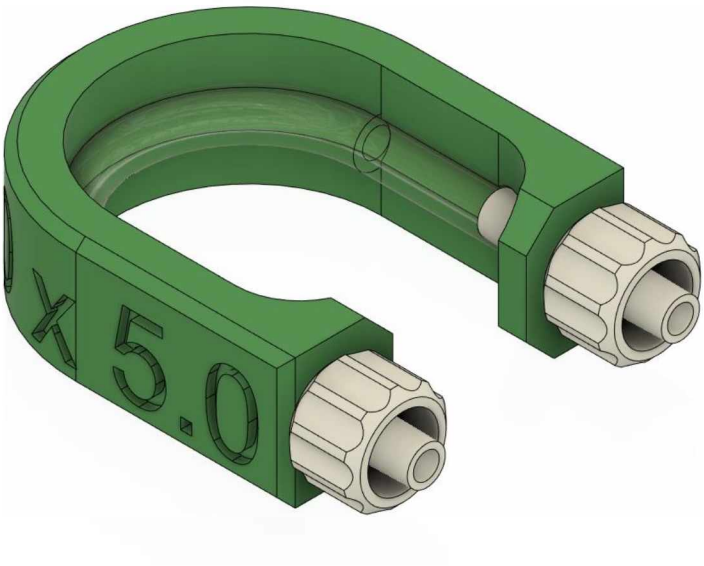

Figure 11: Tubing Cartridge showing cartridge body(green), Luer lock male fittings(white), and tube(clear)

The use of a cartridge allows the ends of the tubing to be fixed in place, by sandwiching the tube between the barb of a Luer-lock fitting and a 3D-printed ring. The cartridge is removable and may be modified to accommodate other tubing sizes. This cartridge also provides the surface

for the rollers to compress the tube against, in order to generate peristaltic action. This cartridge design was designed to flex, such that the cartridge may be inserted in the pumps around the rollers of the cartridge.

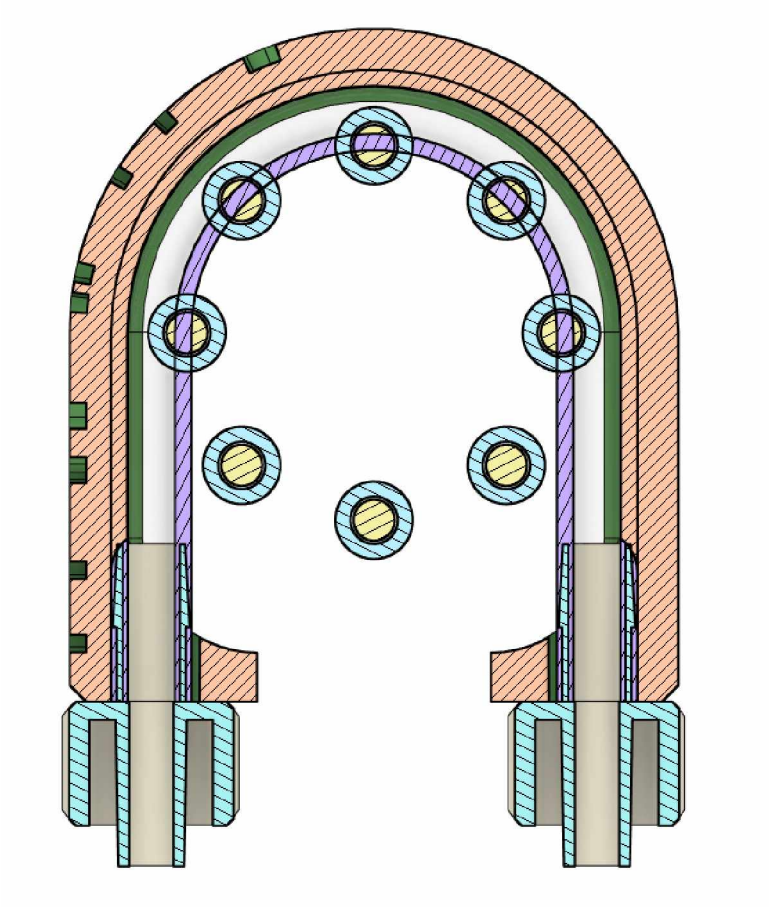

Figure 12: Cross-Section of cartridge design showing cartridge (orange), hose walls (purple), pins and rollers (yellow/cyan), and luer-lock fittings (cyan).

By utilizing a cartridge system, several cascading benefits have been achieved in the entire design. The most notable improvement is that as tubing wears out, it is significantly less complicated to simply remove a cartridge and replace it, than it is completely take the pump apart. By keeping the external geometry of the cartridge the same, especially where the cartridge interfaces with the "wings" of the pump that keep the cartridge fixed in place against the pins, the occlusion of the design, and the wall thickness that it accommodates, can be modified

without having to change any of the other features of the pump. This allows for rapidly changing the use-case of the pumps and allows for having the same pump body be used for a variety of liquids without the concern for mixing parts for one tubing size with the parts for another tubing size.

The cartridge itself is held against the rollers through use of hinged "wings" as shown in Figure 13. These wings are components which can rotate to make ease of accessing the cartridge significantly easier. The inside curve of the wings is concentric to the axis of the rollers, and due to this it keeps the cartridge located without the need for further mechanical registration.

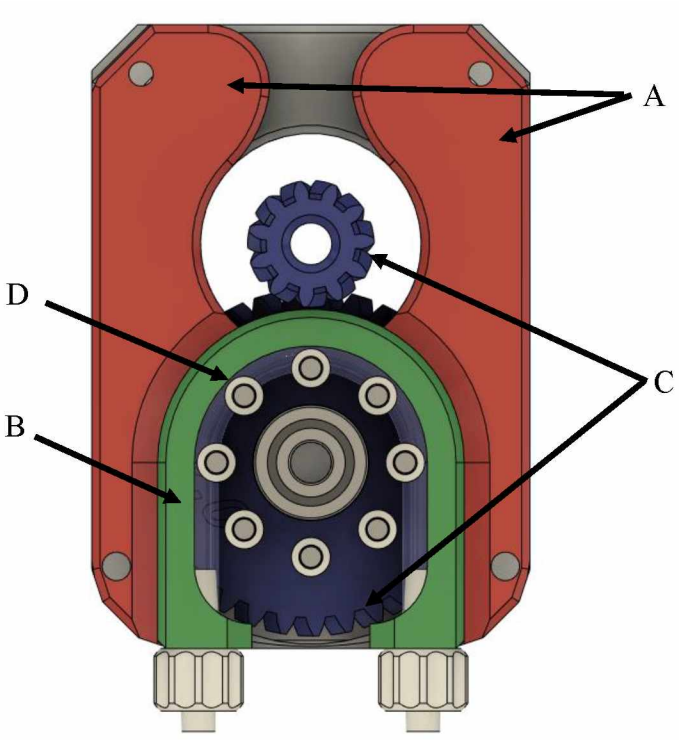

Figure 13: Top view of pump mechanism showing wings (A), cartridge (B), gear mechanism (C), and rollers (D).

Figure 13 shows the wings of the pump in red, and the cartridge in green. Two holes can be seen in each wing, one at the top, and one at the bottom. When assembled, each of these holes has a bolt passing through it, preventing the wings from rotating or translating. However, if the bolts in the bottom of the wings are removed, the wings are free to rotate, allowing access to the

cartridge and the other internal parts of the pump. The cartridge may be pulled out from the side of the pump once the wings have been opened, as shown in Figure 14

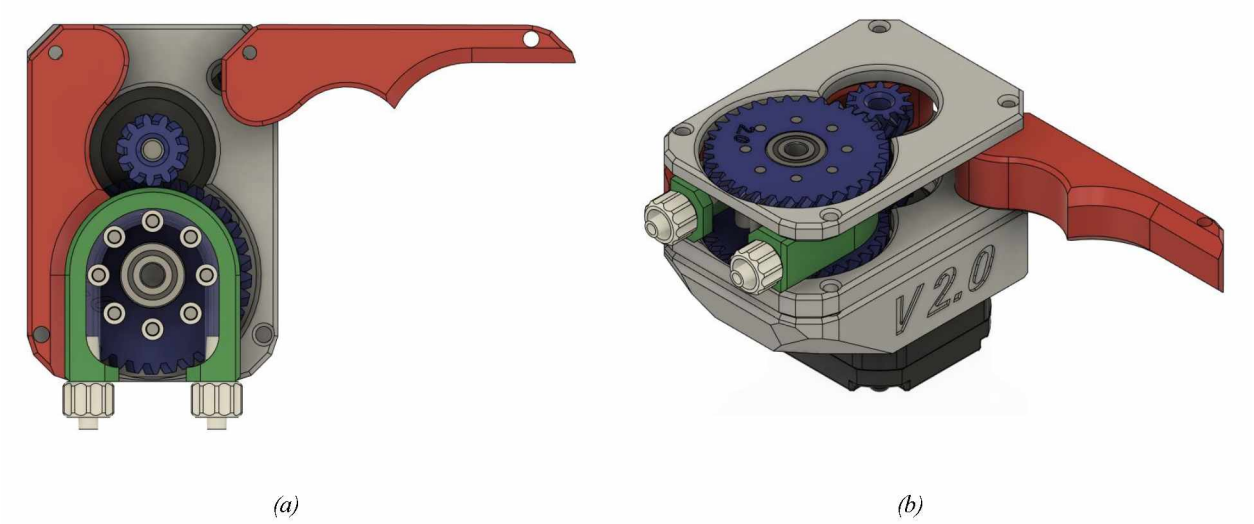

(a) (b)

Figure 14: (a) Top view of pump mechanism showing the right wing opened. (b) Isometric view of pump mechanism showing the right wing opened, and how the cartridge may be accessed when pump is assembled.

3.3 Motor Interchangeability

Another observed issue with the first version of the prototype was a limitation to the maximum speed that the motors could turn. The torque curve of the motors chosen drops off relatively quickly, which would cause the motors to stall. Figure 15 shows the torque curve for the motors as provided by the manufacturer. The motors that were used for this application were the model 14HS13-0804S from manufacturer StepperOnline[25], which is shown in blue in the figure below. This motor had a less desirable performance for torque as the speed increases, and so a different motor choice was made.

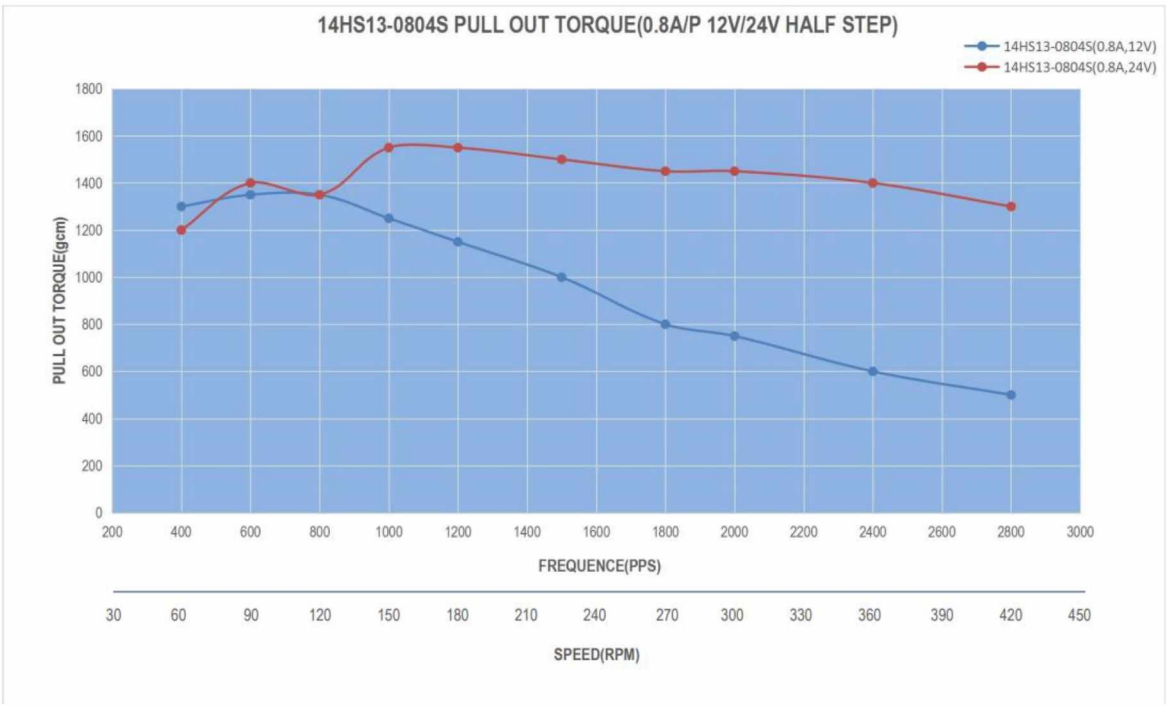

Figure 15: Torque Curve for NEMA 14 Motors chosen [25]

To ensure the maximum flexibility in motor selection, the design for the 2nd version was initially modelled for a NEMA 17 motor, which has a faceplate with holes spaced 42 mm apart. The NEMA 14 motor has a faceplate with holes spaced 35 mm apart, and both NEMA motors selected have square faceplates. Instead of using holes for screws in the pump base, slots were instead used. This allowed for a smaller NEMA 14 motor to be mounted in the same slot as the NEMA 17 motor, without any modification to the hardware.

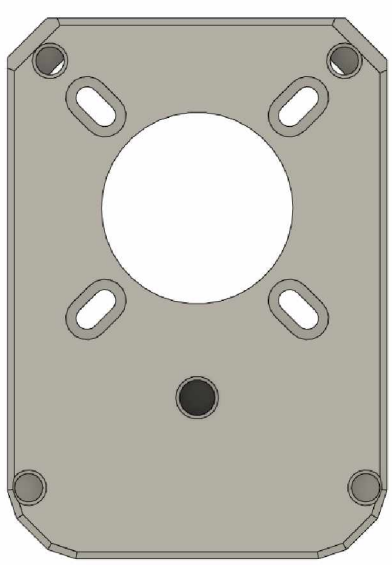

Figure 16: Base of pump body showing slots for mounting screws.

3.4 Electronics and Firmware

The electronics in the first version worked but had significant areas that were worth improving. The 8-bit processor used in the Arduino Mega 2560 has a limited processing power and may cause the pumps to stutter if the processor cannot interpret commands fast enough. The A4988 stepper drivers used were loud and the current could not be easily adjusted. The enclosure also needed to be changed significantly, as the new pumps were larger and used a larger motor, which would not fit in the original mounting slots for the first version.

3.4.1 SKR 2 Control Board

Although the RAMPS controller worked in the first version, an upgrade was justified in this improved design. Since the RAMPS board was released, 32-bit control boards for 3D printers have been released and have quickly come down in price. The improved processing speed of these controllers made them desirable for this new version. To make it easier to upgrade the

pumps, a control board that was compatible with the same firmware was chosen. The SKR 2 board from manufacturer BigTreeTech was chosen for its ease of programming, 32-bit processor, and the ability to use StepStick compatible stepper drivers. Figure 17 shows a plan view of the SKR 2 control board.

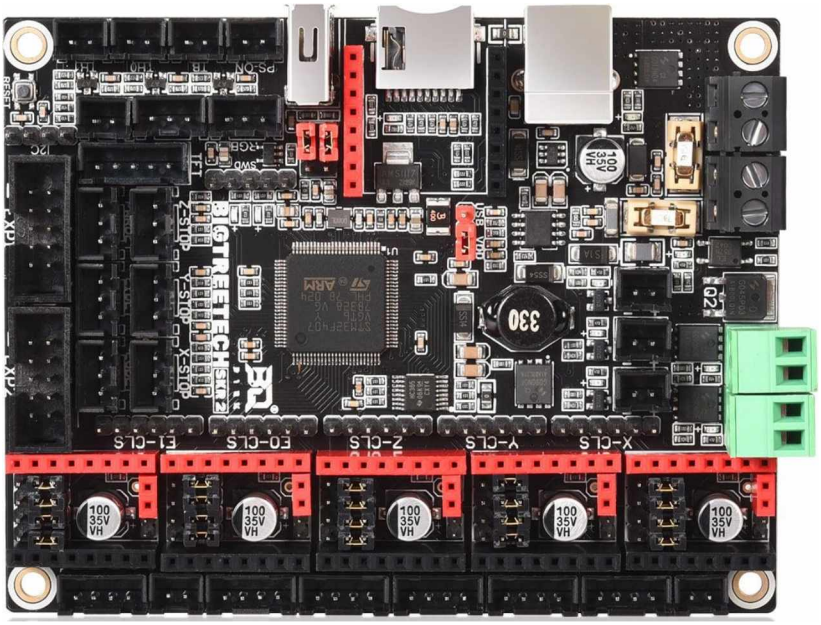

Figure 17: SKR 2 Control Board

The SKR 2 has built-in support for Trinamic stepper drivers such as the TMC2130 and TMC2209, while maintaining backwards compatibility for older stepper drivers such as the A4988. Furthermore, this board is capable of up to five fan outputs (either for cooling electronics, or cooling process fluids), three heater outputs, progress LEDs, and ports to add WiFi control. Nevertheless, this mainboard has a larger footprint than the RAMPS board, but it has a significantly lower vertical dimension. The SKR 2 is a bit more expensive than the RAMPS board, about $35 USD/piece, but the functionality upgrades demonstrated were determined to justify the increased cost [22].

3.4.2 Trinamic TMC2130 Stepper Driver

The Trinamic TMC2130 is a newer stepper motor driver than the A4988, developed by Trinamic Motion Control and is optimized for automated equipment applications. The chip can drive up to 2.5A of current to each output with proper heatsinking and has micro stepping configurable up to 1/256 times. A Trinamic TMC2130 StepStick Module by Biqu industries is shown in Figure 18.

Rather than having the output current determined by a sense potentiometer, the TMC2130 is capable of being controlled with either SPI or UART configuration tools, which allows the current to be set in software rather than physically. The TMC2130 chip has a sophisticated chopper algorithm known as 'StealthChop™', which allows for the motors to run almost entirely silently while still maintaining high motor torque and efficiency.

According to Trinamic, StealthChop "guarantees absolutely quiet motor standstill and silent slow motion, except for noise generated by ball bearings". [16] The chopper can also be configured to utilize spreadCycle™, which is a higher power, dynamic motor control chopper.

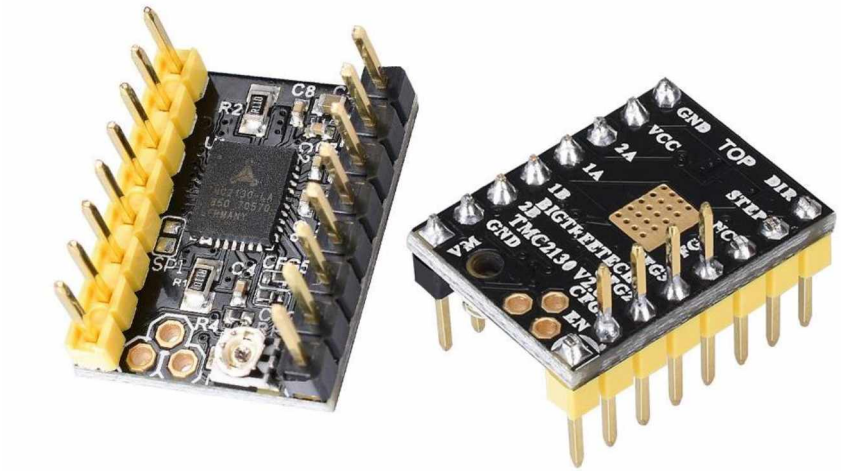

Figure 18: Trinamic TMC2130 StepStick

The TMC2130 includes an integrated current sense circuit, allowing for stall detection to be performed and accounted for in software without any additional modules. This is a new feature to the OSMMPump architecture, allowing the pumps to detect when they have stalled and pause the pump until the user interacts with it. The major downside to utilization of the TMC2130 in this pump is that the drivers are significantly more expensive, by around one order of magnitude. This means that rather than the ~$5 USD that 5 A4988 chips cost, the TMC2130 chips fall into a price bracket around $40 USD for the 5 needed to control the pumps used in the OSMMPump. Similar to the upgraded motherboard, the massive benefits that are present in the TMC2130 chips far outweigh the cost downside to them [27].

3.4.3 Software

To make programming of the pump system easier, a graphical user interface (GUI) was developed. This GUI allows for each pump to be controlled individually. Flow rates, volumes, and duration can all be individually programmed. Additionally, the GUI supports creating flow patterns. This means that pulsing flow can be replicated accurately in the software, as well as time-delayed fluid dispensing.

Figure 19: GUI for programming OSMM Pumps Version 2

Figure 19 shows the first page of the GUI. The programming can be driven by either a combination of flow rate and duration, or output volume and duration. Additionally, the software provides a proportional display of what has been entered. This allows for any discrepancies between entry and intent to be noticed.

3.5 Limitations and Design Deficiencies

This second version of the OSMM Pump, however, still has limitations and areas in the design that may be improved. One of the greatest limitations to this pump design is the materials used. This pump design has been optimized to be 3D printed for all parts that either need to be low friction or come into fluid contact. Most FDM 3D printing materials, such as PLA or PETG have a relatively low glass transition temperature. The prototypes presented in this thesis were printed from eSun PLA+ filament, which has a glass transition temperature of only 53°C [28].

The glass transition temperature is approximately where this material will go from a brittle, glassy solid to a viscous and ductile state. Due to this low glass transition temperature, none of the 3D printed parts used for this research may be used in an autoclave. This limits the usability of this pump in biological assays, as it can only be chemically sterilized. The chemical compatibility of 3D printed materials with common chemical sterilizing agents is not widely documented. Furthermore, the layer lines present in a 3D printed part make it challenging to ensure sterility as these crevices may provide areas for micro-organisms to propagate.

The glass-transition temperature of these common materials provides further challenges with motor selection. Stepper motors tend to heat up significantly during operation and may operate at temperatures of 80 °C higher than ambient temperatures. Due to this heating, the motors tend to soften 3D printed parts they are mounted to and can cause the material to creep significantly over relatively short amounts of time. To prevent this from happening, the motors are run at a much lower current than what they can handle, which limits the amount of torque that they are capable of producing.

Another potential area of improvement for this pump is the installation method of the tubing cartridge. The way the cartridge is installed in this version of the pump may allow for the fittings to come into contact with the rollers, pump body, or gears. Although it is an extremely small area that this may affect, there is still the potential for contamination between these parts. A solution where tubing cartridges may be installed with no contact with any of the mechanical parts would be ideal to prevent any contamination.

Finally, the pumps currently must be programmed on a desktop computer, and then the machine code can be transferred to the pumps themselves. This may be inconvenient and being able to program the machine code on the control system itself may be a boon in many settings.

CHAPTER 4: TESTING RESULTS OF VERSION 2 PUMP

4.1: Testing Methodology

The prototypes were subjected to longevity testing, calibration curve/flow rate testing, and hydrostatic pressure testing. Each of these tests consisted of slightly different setups, but most of them were very similar. As a flow meter precise to individual microliters was not available for the testing, tests needed to run for a long duration in order to collect a significantly measurable sample. All tests only measured bulk material flow and did not factor in the pulsatile nature of the flow, unless otherwise stated.

In the longevity tests, the primary concern was the durability and usability of pumps over an extended duration (up to 10 days of continuous pumping). Additionally, the longevity testing was utilized to gather data for the extremely low flow rates that the pumps are capable of. The pumps were set up to pump at a low flow rate continuously and ran anywhere between five and ten days. To calculate the flow rate, the collection reservoir bottles were weighed before each test began, and weighed again after the test ended. With a given time and the change in mass, a bulk mass flow rate can be estimated by averaging. Subsequently, the volume flow rate can be determined.

The calibration curve/flow rate testing was set up to evaluate how the pumps performed over a variety of flow rates. These tests were a much shorter duration than the longevity tests, running for as short as 10 minutes. The speed for the pump was set and they ran for a specified period. Like the longevity tests, the mass of each bottle was recorded at the beginning of the test and was recorded again after the test concluded.

Pressure testing is the most different of the tests that were conducted. To calculate the pressure that the pumps delivered at a given flow rate, a pressure transducer was utilized to determine the pressure inside a chamber that was sealed other than the inlet mass flow. The

Fluke pressure transducer used outputs 1 mV per unit, and its highest accuracy mode gives an output unit of Pascals. By finding the maximum pressure at a given flow rate, the characteristic curve of the pump could be determined.

Figure 20: Fluke Multimeter (yellow) and pressure transducer unit (black)

4.2 Testing Setup

Low flow rates that are required for testing created inherent challenges to maintain good test procedures. At the low flow rates, without any means of sealing the collection bottles, a significant amount of liquid will evaporate, which will make the results inaccurate. This issue was mitigated by a customized collection reservoir bottles to make tests both easier and more accurate. The customized bottles and collection setups are shown in Figure 21 and Figure 22.

To make the collection of data easier and more accurate, these collection bottles were redesigned. Holes were drilled in the side of clear beverage bottles, toward the bottom. Luer-lock

fittings were then inserted into these holes, and hot glue was used to seal the connection. A stopcock was attached to the valve to make connection of the pumps easier and mess-free. Finally, a small hole was drilled in the lid of the bottles to ensure that air could leave the bottles as liquid was pumped in from the bottom.

Figure 21: Side view of collection bottle, Luer-lock fitting, and stopcock.

To ensure consistent data collection, the hole was placed toward the bottom of the bottle. This ensured that the water being pumped in was consistently below the surface of the mineral oil, without having to insert a hose into the container itself. This arrangement also allowed the water to be drained after tests, while retaining the mineral oil. Previously, the mineral oil was extremely difficult to separate from the water at the end of tests and required pulling a siphon from below the surface of the oil and having to constantly ensure that mineral oil was not being removed as well as the water. By utilizing a stopcock at the base of the bottle, most of the water could be drained while leaving the pool of mineral oil in the bottle, similar to a separatory funnel.

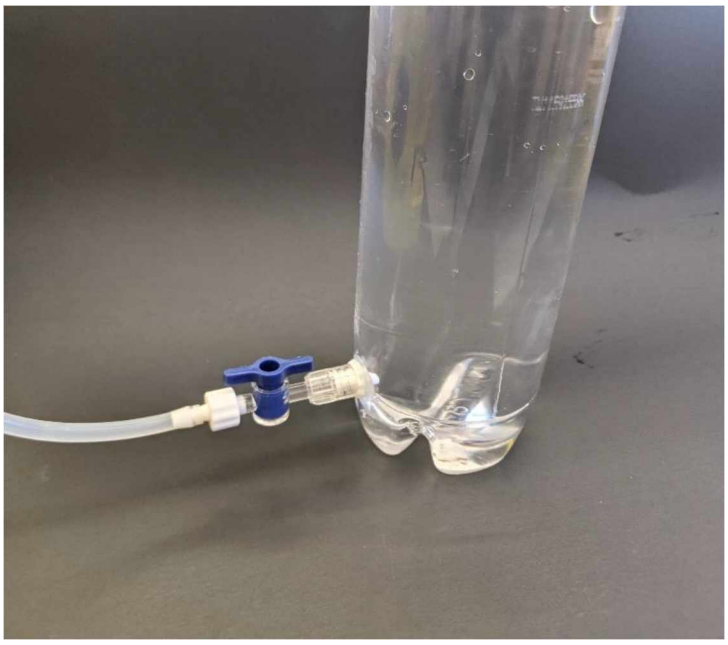

Figure 22: Alternate view of collection bottle, connect to pump tubing

Pressure testing was conducted in a similar manner, overall, but with notable changes. The lid of the bottle was modified to have a pressure transducer inserted into it, which sealed the bottle. Rather than needing a pool of mineral oil, these tests could be conducted with only water in the bottle. Finally, it was highly important that the bottle be sealed for these tests to measure pressure accurately, so care was taken to ensure this by reinforcing all seals with additional thermoplastic adhesive. During pressure testing these seals leaked occasionally, which lead to that test needing to be repeated once the bottle was replaced or the seals were repaired.

Figure 23: Pressure transducer assembly showing transducer (top), adapter fittings (middle), and collection bottle (bottom).

The fluid inlet was maintained at the bottom of the bottle, and filled gradually, increasing the pressure. Due to the compressibility of the air in the bottle, it is desirable to almost fill the bottle completely with liquid before pressure testing begins. This decreases the amount of time that the pressure test may take.

4.3 Test Results

4.3.1 Pump Calibrations

In the flow rate calibration curves, a very consistent linear trend is seen, showing a linear increase in flow rate corresponding with a linear increase in the motor speed. These curves may be used to calibrate the pumps, by using the slope of the line to adjust how many steps the motor will turn for one microliter of fluid delivered. The curves for the three pumps that were tested are shown in Figure 24, and the regression equations and correlation coefficient R^2 are shown in The x-axis shows the flow rate that the pumps were told to move (in µL/min), but this number is entirely uncalibrated. The y-axis shows the averaged output flow rate of the pumps. A perfectly calibrated pump would have a curve with a slope of 1, but the uncalibrated pump follows Eq. 4. The pumps can be calibrated by multiplying the input command to the pumps by $1/m$.

$$y = mx \qquad \text{Eq. 4}$$

Table 4.1: Regressions of three pumps in calibration tests

Pump	Regression Equation	Correlation Coefficient R^2
A	$y = 11.9466x$	0.99955
B	$y = 13.4617x$	0.99719
C	$y = 8.1852x$	0.99965

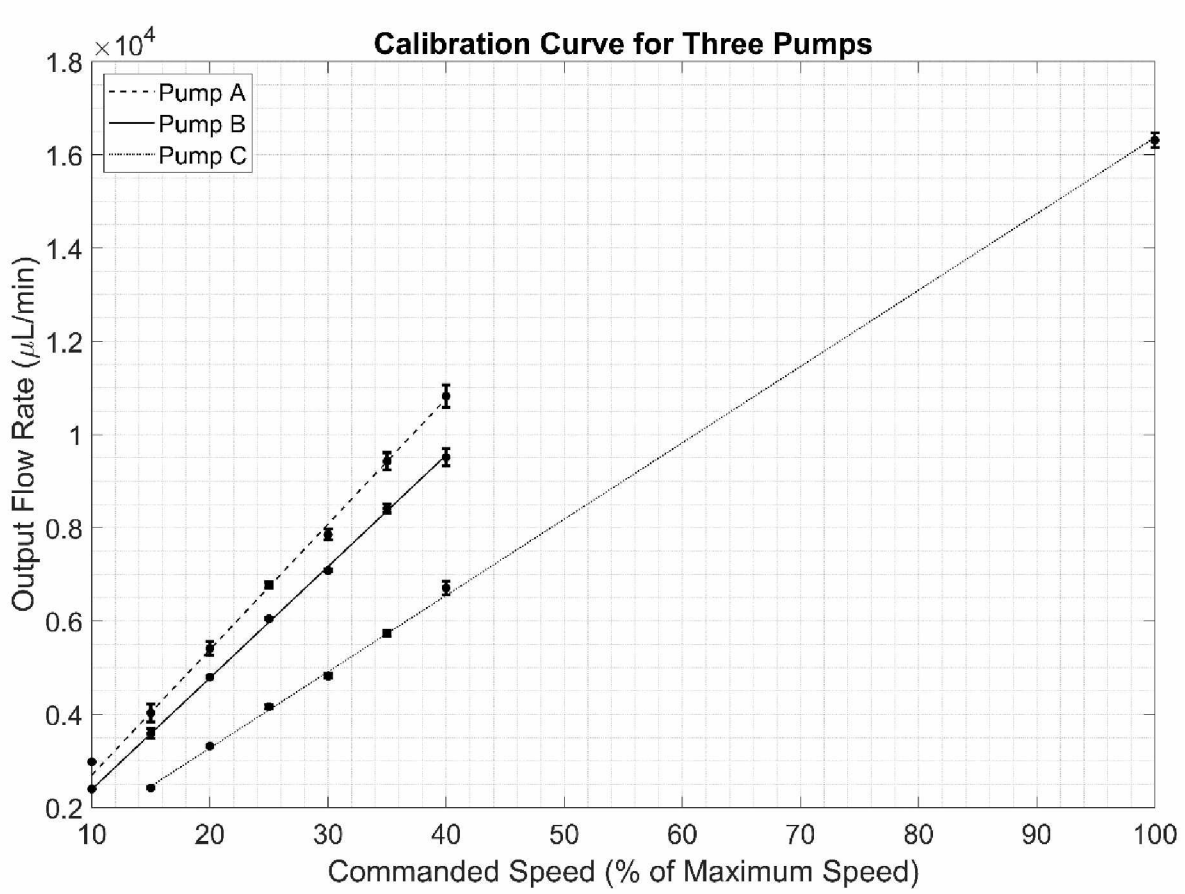

Figure 24: Flow Rate Calibration Results for three pumps.

The linearity of the curves indicates highly consistent pump operation and no increase in error as the speed of the pumps increase. These tests were conducted over a range from a commanded speed of 300 to 800 in steps of 100. Each data point represents the average of 6 tests in which one standard deviation is represented by the error bar in Figure 24. The approximate range of actual flow rates in this range was approximately 2 mL/min to 10 mL/min. This range was primarily chosen to reduce the time that testing took, with a greater amount of data being desirable. In order to evaluate whether extrapolations may be made from this curve fit, the curve for pump C was used to predict performance at an input speed of 2000, which was just under the stall speed of these motors. The linear regression predicted that at a speed of 2000, the output flow rate would be 16.485 mL/min. Over six tests at that input speed, the mean output flow rate

was 16.313 mL/min. The error between the predicted and the actual output was calculated at only 1.05%.

4.3.2 Long-Term Low Flow Tests

In these tests, the goal was to see an extremely low average flow rate that was ideally extremely consistent between tests. This was measured in the same way as the tests conducted on the first version pumps, following Eq. 3. Due to the 10-day length of these long-term tests, a limited amount of data was collected. Each pump was to be tested 5 times over a period of ten days per test, but some data was lost due to experimental setup errors. Figure 25 presents the data from these longevity tests. Pump 1 has a noticeable outlier for test #2, as the data is relatively consistent otherwise. Thus, the data for test #2 was ignored in the analysis. Pump 2 was the most consistent of the three tested, with its data showing a near-perfect horizontal line and variances of less than one μL/min flow rate. Pump 3 was still relatively consistent, but had a range from 7.8 to 9.5 μL/min. Summary statistics for these tests are presented below in Table 4.2. This data shows that although the flow is pulsatile over very short time spans, the flow is extremely consistent both between tests and over a period of days.

Table 4.2: Summary Statistics for Longevity Tests

Pump	Average Flow Rate (μL/min)	Coefficient of Variation
1	12.63	2.484%
2	13.73	0.867%
3	8.93	6.914%

**The average flow rate was calculated as the change in volume over the duration of the test. Coefficient of Variation is defined as one standard deviation divided by the mean.*

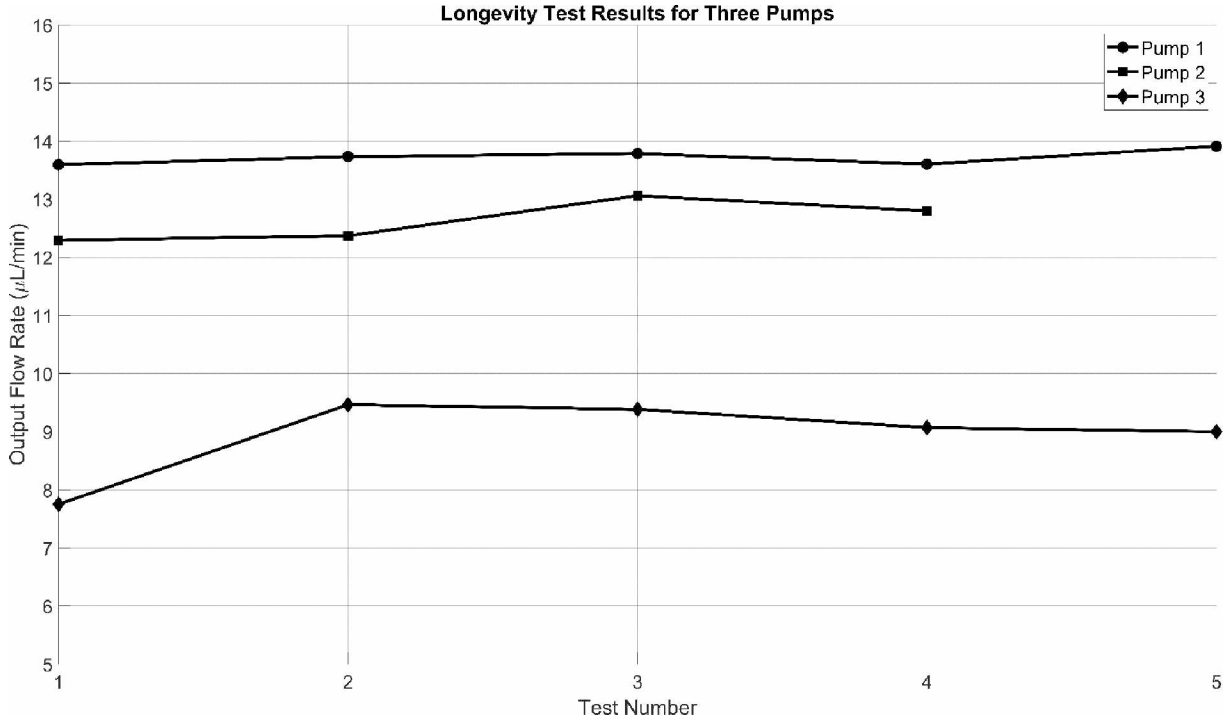

Figure 25: Longevity Test Results for Pumps 1, 2, and 3

In addition to the specific data usefulness of the longevity tests, they were also useful as a durability study of the pumps themselves. Although a mostly qualitative analysis, some consistent trends were observed. The biggest observation from this testing was that proper setup of the pumps themselves was highly important. If the electrical current setting for the pumps was not correct, they would heat up significantly and cause the 3D printed parts to deform, which could ruin the test. The parts that tended to have the most issues with this were the motor mount, which all other pieces are mounted to, and the drive gear. The drive gear was the most common failure point on these pumps, as it would either soften from the motor heat, or more commonly, the threads on the gear would strip out. The drive gear is held onto the motor shaft by two 3-mm diameter grub screws. Since the threads of these screws is relatively fine, the pressure on the threads is high. This caused the plastic to creep over the constant stress of the longevity tests.

Additionally, wear in the silicone tubing was observed. Wear was to be expected due to using thin wall tubing not intended from the manufacturer for peristaltic pumps. A wear-in period of approximately one day of consistent use was observed, after which the peristaltic effect decreased, but became more consistent. As the tubing continued to wear, a common weak point was found where the tubing was sandwiched between the cartridge and the fittings. This point would occasionally tear when changing cartridges, but only after weeks of using the pumps for testing constantly. All long-term low-flow tests were conducted with the same tubing in each pump, showing that the tubing in the pumps only needs to be replaced over a period of approximately two months of use(at a low flow rate). This mechanical wearing would be expected to occur much faster if the pumps are running at higher speeds.

4.3.3 Pressure Testing

Figure 26 shows a setup for the pressure testing. The pressure transducer recorded data at location P_3. As Pressure P_3 underestimates the actual pump pressure P_m because of both the hydraulic head from the height of fluid h, and the head loss in the tubing leading into the bottle, below we derive a formula to estimate P_m based on the measured P_3.

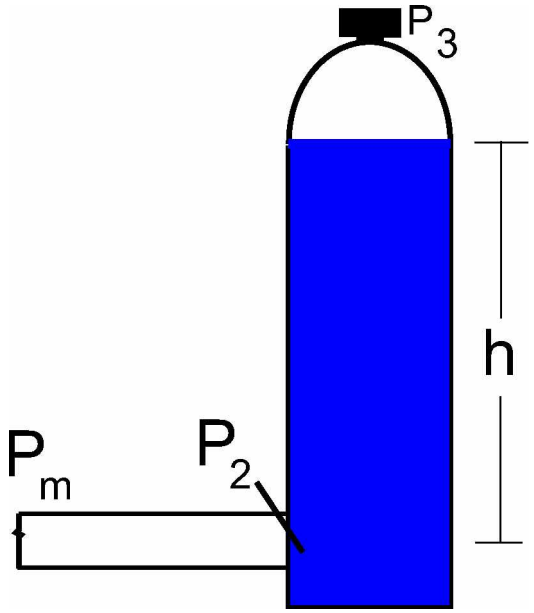

Figure 26: Diagram of bottle setup for pressure tests.

Pressure loss in a closed channel is characterized by the Darcy-Weisbach equation:

$$h_f = f\left(\frac{L}{D}\right)\left(\frac{V^2}{2g}\right) \quad \text{Eq. 5}$$

$$f = \frac{64}{R_e} \quad \text{Eq. 6}$$

$$R_e = \frac{VD}{\nu} \quad \text{Eq. 7}$$

$$P_b = \rho g h_f \quad \text{Eq. 8}$$

In Eq. 5, f is the Darcy-Weisbach friction factor (as given in Eq. 6), L is the length of the channel, D is the diameter of the channel, ν is the dynamic viscosity of the flow, V is the average speed of the flow in the closed channel, and g is the gravitational acceleration. The Reynold's number *Re* used in calculating the friction factor is calculated by Eq. 7. Note that values of the Reynold's number below 2000 are understood to be laminar. Eq. 8 relates the head loss h_f to the backpressure P_b by the density of the fluid ρ and gravitational acceleration.

The Darcy-Weisbach equation is valid for laminar, developed flows. Per the dimensions of the tubing used in our pressure testing, and the averaged flow speed obtained from earlier testing, the Re number calculated falls in the range of [1.458, 116.6]. Therefore, the Darcy-Weisbach equation can be used here to approximate the head loss of flow through the tubing of the peristaltic pump.

The hydrostatic pressure difference between P_2 and P_3 is given by Eq. 9, where ρ is the density of the fluid, g is the gravitational acceleration, and h is the vertical distance between the two points being measured. These tests were conducted with a head height of 16.5 cm and used deionized (DI) water as the process fluid. The hydrostatic pressure difference was found to be generally insignificant in comparison to pressure loss in the tubing itself, at only 1.62 kPa.

$$\Delta P = \rho g h \qquad \text{Eq. 9}$$

$$P_m = P_3 + \rho\left(gh + f\left(\frac{L}{D}\right)\left(\frac{v^2}{2}\right)\right) \qquad \text{Eq. 10}$$

The outlet pressure of the pump can be estimated by Eq. 10. This equation does not factor in minor loss coefficients due to fittings, as that pressure loss was determined to be insignificant. The pressure at the motor outlet P_m, as well as the pressure loss due to the tubing and the measured pressure P_3 are shown in Figure 27. At flow rates above 12,000 µL/min, the backpressure from friction in the tubing is almost half of the pressure that was measured at point P_3. This demonstrates that at relatively high flow rates, the pressure drop in channels is not inconsiderable. The tubing that was used in this testing was of extremely large internal diameter, compared to most microfluids analysis. If the same flow rate were to be maintained in a channel only 10 times smaller inner diameter (0.3mm), the backpressure would increase by a factor of 1,000. Thus, most microfluids applications will make use of lower volumetric flow rates since generating these high pressures is infeasible.

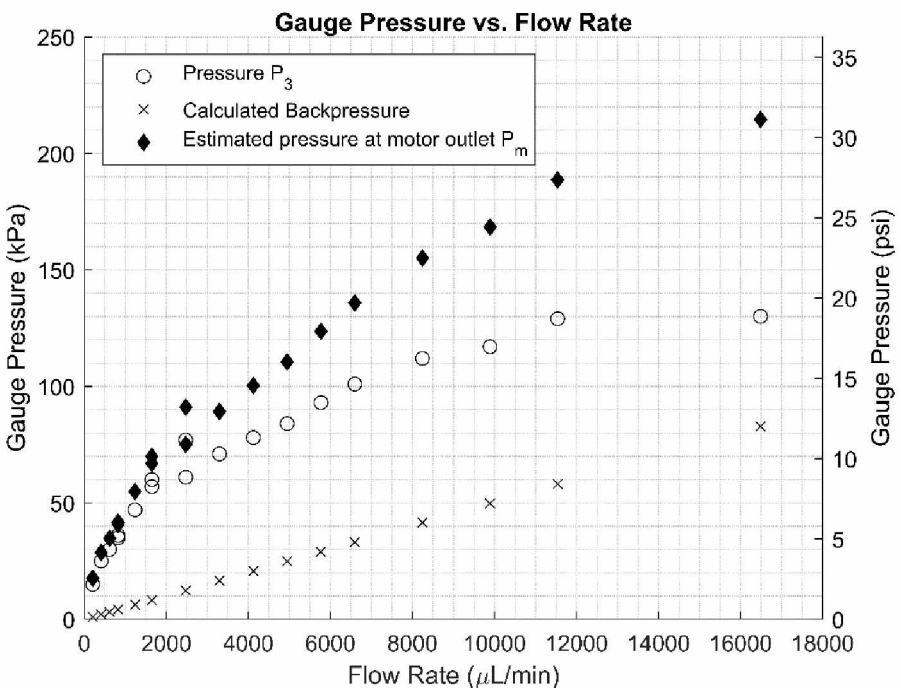

Figure 27: Calculated and Measured Pressure.

CHAPTER 5: CONCLUSIONS AND FUTURE WORK

5.1 Conclusions

The feasibility of a 3D printed microfluids pump was demonstrated in two distinct prototypes. Each design was shown to be reliable over multiple days of pumping with little to no meaningful wear on the 3D printed parts. The second version of the prototype aimed to solve some of the issues with the first version, namely the usability challenges with inserting and changing the pump tubing, as well as being able to interconnect the pumps with microfluids devices. The pumps were shown to be able to maintain flow rates in the range of 10s of μL/min, all the way up to flow rates in the range of 10s of mL/min. These pumps were also shown to be able to generate and sustain pressures of up to 130 kPa gauge pressure, or almost 20psi.

Open-source lab equipment has been a rapidly growing area of research for years, with many goals to be decreased cost barrier to entry and easy configurability. Many of these designs are modular or semi-modular and allow for a variety of tubing sizes and configurations. The low-cost aspect of developing open-source lab equipment has been explored. The pumps presented here fall in an extremely low price bracket of $10-$20 per pump, making them readily available. The designs presented here do not require any specialized equipment other than a 3D printer, and only use readily available prefabricated parts such as motors, shafts, and bearings.

The updated second version of this design also incorporates the use of standard Luer-lock fittings, a feature not seen in other common open-source pump designs. This allows for the ready interconnection of a variety of equipment, from probe needles to syringes to large reservoirs. These fittings are designed for use in the medical industry and as such have wide compatibility with many of the tools used in microfluids analysis.

The current design of the OSMM pump is suitable for research laboratory environments, where sterility is not necessary, but a repeatable high-precision pump is. The ability to produce parts in house greatly reduces both the cost to the user, and the need to have qualified technicians install replacements. These pumps may be printed in different materials in accordance with the requirements of the individual users and may also be readily modified for further niche cases. Although the pumps could be developed further into commercialization as an off-the-shelf product, that would be antithetical to the goals of this project.

5.2 Future Work

There are numerous future studies that may be conducted based on the results from these new pumps. One of the largest areas of interest is establishing a profile of the pulse size and patterns of these pumps in order to have a more thorough understanding of the flow behavior. Another potential area of research involves miniaturization of these pumps, such that they can be readily integrated into more assays.

The design of these pumps still has further optimization to improve reliability and usability. As mentioned in the testing section, one of the most observed issues was the motors heating up and causing the 3D printed parts to deform. This might be solvable in one of two ways- Reducing the current to the motors, as was done here; Printing the parts in a plastic with greater dimensional stability at elevated temperatures, such as Nylon copolymer; or optimizing the design so that the pumps may operate in the low flow rate range demonstrated here without heating up as much. Stepper motors tend to run the most efficiently at higher speeds, and will conversely heat up and run less efficiently at low speeds. To achieve the low flow presented here while allowing the pumps to run most efficiently, using a tube with a smaller inner diameter would be feasible. This would limit the maximum flow rate achievable by these pumps, but this

is not a concern for most applications. In the current configuration, the OSMM pump may pump at flow rates up to 16 mL/min, which is no less than two orders of magnitude faster than what most microfluidic assays require.

Additionally, the OSMM pump design may be optimized to be more readily usable in clinical environments. The current design may not be sterilized in an autoclave, as the PLA copolymer used will simply melt. Very few 3D printable materials will successfully endure an autoclave, so modifying the design such that the tubing can be more readily removed for sterilization would be desirable. Additionally, the process of 3D printing leaves parts with a surface that can readily harbor bacteria and other microorganisms, due to the ridges left behind as the layers are stacked up. However, developing this pump system more towards a clinical product reduces the open-source nature of being able to produce these pumps in-house, and this tradeoff must be carefully weighed.

References:

[1] D. Sabourin *et al.*, "The MainSTREAM Component Platform: A Holistic Approach to Microfluidic System Design," *Journal of Laboratory Automation*, vol. 18, no. 3, pp. 212–228, Jul. 2013, doi: 10.1177/2211068212461445.

[2] E. T. da Costa, M. F. Mora, P. A. Willis, C. L. do Lago, H. Jiao, and C. D. Garcia, "Getting started with open-hardware: Development and control of microfluidic devices," *Electrophoresis*, vol. 35, no. 16, pp. 2370–2377, 2014, doi: 10.1002/elps.201400128.

[3] T. Baden, A. M. Chagas, G. Gage, T. Marzullo, L. L. Prieto-Godino, and T. Euler, "Open Labware: 3-D Printing Your Own Lab Equipment," *PLoS Biology*, vol. 13, no. 3, Mar. 2015, doi: 10.1371/journal.pbio.1002086.

[4] E. N. Aitavade, S. D. Patil, A. N. Kadam, and T. S. Mulla, "An Overview of Peristaltic Pump Suitable For Handling of Various Slurries and Liquids," SICETE. [Online]. Available: www.iosrjournals.org

[5] C. K. Byun, K. Abi-Samra, Y. K. Cho, and S. Takayama, "Pumps for microfluidic cell culture," *Electrophoresis*, vol. 35, no. 2–3. Wiley-VCH Verlag, pp. 245–257, Feb. 01, 2014. doi: 10.1002/elps.201300205.

[6] D. J. Beebe, G. A. Mensing, and G. M. Walker, "Physics and applications of microfluidics in biology," *Annual Review of Biomedical Engineering*, vol. 4. pp. 261–286, 2002. doi: 10.1146/annurev.bioeng.4.112601.125916.

[7] K. S. Elvira, X. C. I Solvas, R. C. R. Wootton, and A. J. Demello, "The past, present and potential for microfluidic reactor technology in chemical synthesis,"

Nature Chemistry, vol. 5, no. 11. pp. 905–915, Nov. 2013. doi: 10.1038/nchem.1753.

[8] "MP2 Stand Alone Peristaltic Pump," *MEINHARD*. https://www.meinhard.com/Shop-by-Product/Peristaltic-Pumps/MP2-Stand-Alone-Peristaltic-Pump/ (accessed Feb. 02, 2022).

[9] A. Jönsson, A. Toppi, and M. Dufva, "The FAST Pump, a low-cost, easy to fabricate, SLA-3D-printed peristaltic pump for multi-channel systems in any lab", doi: 10.17605/OSF.IO/3R7H4.

[10] T. Ching *et al.*, "Highly-customizable 3D-printed peristaltic pump kit," *HardwareX*, vol. 10, Oct. 2021, doi: 10.1016/j.ohx.2021.e00202.

[11] "Guide to Stereolithography(SLA) 3D Printing," *Formlabs*. https://formlabs.com/blog/ultimate-guide-to-stereolithography-sla-3d-printing/ (accessed Jan. 09, 2022).

[12] M. R. Behrens *et al.*, "Open-source, 3D-printed Peristaltic Pumps for Small Volume Point-of-Care Liquid Handling," *Scientific Reports*, vol. 10, no. 1, Dec. 2020, doi: 10.1038/s41598-020-58246-6.

[13] T. Bayraktar and S. B. Pidugu, "Characterization of liquid flows in microfluidic systems," *International Journal of Heat and Mass Transfer*, vol. 49, no. 5–6. Elsevier Ltd, pp. 815–824, 2006. doi: 10.1016/j.ijheatmasstransfer.2005.11.007.

[14] D. F. Elger, B. A. Lebret, C. T. Crowe, and J. A. Roberson, *ENGINEERING FLUID MECHANICS*, 11th ed. Wiley, 2016.

[15] C.-F. Chen and K. L. Drew, "Droplet-based microdialysis-Concept, theory, and design considerations," *Journal of Chromatography A*, vol. 1209, no. 1–2, pp. 29–36, Oct. 2008, doi: 10.1016/j.chroma.2008.09.006.

[16] C.-F. Chen and K. Drew, "Droplet-based digital microdialysis," US20090107907A1, Apr. 30, 2009

[17] M. P. McIntyre, G. van Schoor, K. R. Uren, and C. P. Kloppers, "Methodologies towards approximating the volume displacement by a roller in a roller-type peristaltic pump," *Sensors and Actuators A: Physical*, vol. 335, Mar. 2022, doi: 10.1016/j.sna.2022.113379.

[18] "Capricorn Premium 3D Printing Accessories-Low Friction 1.75mm Bowden Tubing," *Capricorn*. https://www.captubes.com/shop/#!/1-Meter-XS-Low-Friction-1-75mm-Bowden-Tubing/p/82190682/category=23214267 (accessed Jan. 10, 2022).

[19] M. Watanabe and H. Yamaguchi, "THE FRICTION AND WEAR PROPERTIES OF NYLON*," 1986.

[20] D. Jenke, "Evaluation of the chemical compatibility of plastic contact materials and pharmaceutical products; safety considerations related to extractables and leachables," *Journal of Pharmaceutical Sciences*, vol. 96, no. 10. John Wiley and Sons Inc., pp. 2566–2581, 2007. doi: 10.1002/jps.20984.

[21] "Needle Gauge Chart," *Hamilton Company*, 2022. https://www.hamiltoncompany.com/laboratory-products/needles-knowledge/needle-gauge-chart (accessed Jan. 12, 2022).

[22] RepRap user "johnnyr," "Arduino Mega Pololu Shield," Nov. 20, 2018.

[23] Joem, "StepStick," 2011. https://reprap.org/mediawiki/index.php?title=StepStick&oldid=30316 (accessed Oct. 11, 2021).

[24] "Small-bore connectors for liquids and gases in healthcare applications -- Part 7: Connectors for intravascular or hypodermic applications," May 2021.

[25] "Nema 14 Bipolar 1.8deg 18Ncm 0.8A 5.4V 35x35x34mm 4 wires," *StepperOnline*. Oct. 30, 2020.

[26] "BIGTREETECH SKR 2 Control Board 32 Bit Upgrade SKR V1.4 Turbo Motherboard TMC2208 TMC2209 Drive For CR10 Ender 3 V2.0 3D Printer," *BigTreeTech*, 2021. https://www.biqu.equipment/products/bigtreetech-skr-2?variant=39285016363106 (accessed Jan. 12, 2022).

[27] "TMC2130 DATASHEET," *TRINAMIC Motion Control GmbH & Co. KG.* TRINAMIC Motion Control GmbH & Co. KG, Jun. 12, 2021. [Online]. Available: www.trinamic.com

[28] "PLA+," Nov. 2021. [Online]. Available: www.esun3d.net

Appendix

OSMM Pump Bill of Materials (BOM)

The bill of materials (BOM) has been broken into separated BOMs for an individual pump unit, as well as the BOM for the electronics and electronics enclosure. Each BOM contains two tables: prefabricated parts, and 3D printed parts.

Table A.1: OSMM Pump unit Prefabricated Parts BOM

Part	Source	Unit Cost	Quantity	Total Cost
605ZZ Radial Ball Bearing	https://www.ebay.com/itm/193259006072	$0.785	2	$1.57
5x36mm steel shaft	https://www.mcmaster.com/91595A380/	$0.66	1	$0.66
3mmIDx5mmOD silicone tubing	www.amazon.com/dp/B07PPWJYQZ	$6.49	1	$6.49
Male Luer-Lock fittingx1/8" hose barb	www.amazon.com/dp/B003NV2T34	$0.62	2	$1.24
#4x3/16"x0.5" Nylon Screw Spacers	https://www.mcmaster.com/94639A714/	$0.12	6	$0.72
2.5x25mm steel dowel pins	www.amazon.com/uxcell-Stainless-Cylindrical-Support-Elements/dp/B07Y58TLDS/	$.27	6	$1.60
NEMA 17 Motor	https://www.omc-stepperonline.com/nema-17-stepper-motor/nema-17-bipolar-42ncm-59-49oz-in-1-5a-42x42x39mm-4-wires-w-1m-cable-and-connector.html	$8.99	1	$8.99
M3x0.5x35mm cap head screws	www.ebay.com/itm/112016567172	$0.487	4	$1.95
M3x0.5 hex nut	https://www.ebay.com/itm/383536842492	$0.04	4	$0.16
M3 Heat-Set threaded inserts	www.amazon.com/B087NBYF65	$0.14	4	$0.56

Table A.2: OSMM Pump unit 3D printed parts

Part Name	Quantity
Pump Base	1
Lower gear cover	1
Cartridge Wing	2
Drive gear	1
Roller gear	2
Upper Gear Cover	1
Tube cartridge	1
Tube lock	1
Bolt knob	4